The preferred upconversion pathway for the red emission of lanthanide-doped upconverting nanoparticles, $NaYF_4$:Yb^{3+},Er^{3+}

Taeyoung Jung,[‡a] Hong Li Jo,[‡a] Sang Hwan Nam,[‡b] Byeongjun Yoo,[c,d] Youngho Cho,[e] Jongwoo Kim,[b] Hyung Min Kim,[e] Taeghwan Hyeon,[c,d] Yung Doug Suh,[b,f] Hohjai Lee,[*a] Kang Taek Lee[*a]

[a] Department of Chemistry, Gwangju Institute of Science and Technology (GIST), Gwangju 500-712, Korea. E-mail: ktlee@gist.ac.kr, hohjai@gist.ac.kr; Tel: (+82) 62-715-3685

[b] Laboratory for Advanced Molecular Probing (LAMP), Korea Research Institute of Chemical Technology, Daejeon 305-600, Korea.

[c] Center for Nanoparticle Research, Institute for Basic Science (IBS), Seoul 151-742, Korea.

[d] School of Chemical and Biological Engineering, Seoul National University, Seoul 151-742, Korea.

[e] Department of Bio & Nano Chemistry, Kookmin University, Seoul 136-702, Korea.

[f] School of Chemical Engineering, Sungkyunkwan University, Suwon 440-746, Korea.

[‡] T. Jung, H. L. Jo, S. H. Nam contributed equally to this work

[†]Electronic Supplementary Information (ESI) available: Details of reagents, synthetic procedure, characterization and spectroscopy of UCNPs. See DOI: 10.1039/c000000x/

Lanthanide-doped upconverting nanoparticles (UCNPs, $NaYF_4:Yb^{3+},Er^{3+}$) are well known for emitting visible photons upon absorption of two or more near-infrared (NIR) photons through energy transfer from the sensitizer (Yb^{3+}) to the activator (Er^{3+}). Of the visible emission bands (two green and one red band), it has been suggested that the red emission results from two competing upconversion pathways where the non-radiative relaxation occurs after the second energy transfer (pathway A, $^4I_{15/2} \rightarrow {}^4I_{11/2} \rightarrow {}^4F_{7/2} \rightarrow {}^2H_{11/2} \rightarrow {}^4S_{3/2} \rightarrow {}^4F_{9/2} \rightarrow {}^4I_{15/2}$) or between the first and the second energy transfer (pathway B, $^4I_{15/2} \rightarrow {}^4I_{11/2} \rightarrow {}^4I_{13/2} \rightarrow {}^4F_{9/2} \rightarrow {}^4I_{15/2}$). However, there has been no clear evidence and thorough analysis on the partitioning between the two pathways. We examined the spectra, power dependence, and time profiles of UCNP emission by either 980-nm or 488-nm excitation, to address which pathway is preferred. It turned out that the pathway B is predominant for the red emission over a wide range of excitation power.

UCNPs are regarded as the most promising imaging probes thanks to their unique optical properties.[1–5] Their emission wavelengths are shorter than the excitation wavelength as a result of the "upconversion" process. Owing to this optical property as well as their photo-stability (*i.e.*, non-blinking and non-bleaching emission), and the non-invasive NIR light source used for excitation (*e.g.*, 980-nm diode laser), UCNPs recently attracted enormous attraction even in the fields of biomedical diagnosis and therapeutics beyond biological imaging.[6–11] The most popular UCNP system, $NaYF_4:Yb^{3+},Er^{3+}$, has three major emission bands in the visible spectral range, centered at 525 nm (green), 540 nm (green), and 655 nm (red). The generally accepted energy level diagram of UCNPs (hexagonal phase β-$NaYF_4:Yb^{3+},Er^{3+}$ or β-$NaYF_4:Yb^{3+},Er^{3+}/NaYF_4$ with a non-luminescent shell) as well as the energy flow representing the upconversion are shown in Figure 1.[12] A Yb^{3+} in the UCNP crystal absorbs a 980-nm photon, and is excited to the $^2F_{5/2}$ state. Then the excitation energy is transferred to an adjacent Er^{3+}, which leads to the population of the $^4I_{11/2}$ state. Subsequently, an additional energy transfer occurs from another Yb^{3+} to the Er^{3+}, resulting in further excitation of Er^{3+} to the higher level, $^4F_{7/2}$. After non-radiative multiphonon relaxation to one of the three states that are slightly lower in energy ($^2H_{11/2}$, $^4S_{3/2}$, and $^4F_{9/2}$), the Er^{3+} emits one visible photon (*ca.* 525, 540, or 655 nm, respectively) (Figure 1). This pathway denoted by "A" involves the transitions in Er^{3+}, $^4I_{15/2} \rightarrow {}^4I_{11/2} \rightarrow {}^4F_{7/2} \rightarrow {}^2H_{11/2}$ (green), $^4S_{3/2}$ (green), $^4F_{9/2}$ (red) $\rightarrow {}^4I_{15/2}$. As for the red emission (655 nm), however, an alternative pathway was suggested, where the non-radiative multiphonon relaxation occurs from the intermediate excited state of Er^{3+} ($^4I_{11/2}$) to a lower-energy state ($^4I_{13/2}$) immediately after the first energy transfer.[13–20] This is followed by the second energy transfer and excitation of Er^{3+} to the $^4F_{7/2}$ state (Figure 1). This pathway denoted by "B" involves the transitions in Er^{3+}, $^4I_{15/2} \rightarrow {}^4I_{11/2} \rightarrow {}^4I_{13/2} \rightarrow {}^4F_{9/2} \rightarrow {}^4I_{15/2}$. Although the same electronic state ($^4F_{9/2}$) is populated prior to the red emission in both mechanisms, the pathways up to that point are totally different. However, there has been no clear experimental evidence that shows quantitative partitioning into these distinct channels. Most recently, the mechanism of upconversion has been revisited by Anderson *et al.*,[21] where they proposed a new mechanism for the origin of the red emission. In this paper, we stick to the traditional mechanisms and point out that some modification is necessary.

The UCNP system we studied the photophysics about was hexagonal *β*-$NaYF_4$:Yb^{3+},Er^{3+}/$NaYF_4$ with the diameter of *ca.* 30 nm, which were synthesized by the same procedure as in our previous work.[12] The dopant ions, Yb^{3+} and Er^{3+}, with oxidation number of +3 occupy the sites for the Y^{3+} in the crystal and therefore the charge is fully compensated.

In an effort to figure out whether the non-radiative multiphonon relaxation occurs through the pathway A or B, we excited Er^{3+} in UCNPs directly with 488-nm laser. The commercially available 488-nm laser provides nearly exact second harmonic of 980 nm. Therefore, with 488-nm one photon excitation, one can directly excite Er^{3+} to $^4F_{7/2}$ state, which is equivalent to the two-photon excitation with 980 nm on the pathway A. On the other hand, the pathway B is bypassed with 488-nm excitation. In Figure 2, the upconversion emission spectrum obtained by 980-nm excitation (Figure 2a) is compared to that obtained by one-photon excitation with 488 nm (Figure 2b). Upon 488-nm one-photon excitation, the red band nearly disappeared in stark contrast to that in the original spectrum obtained by the 980-nm two-photon upconversion excitation. This remarkable difference between the two spectra indicates that the red emission is barely produced when the upconversion pathway A is available while B is bypassed. On the other hand, as for the green emission, the intensity is preserved in this excitation scheme because its origin is obviously the pathway A. We also note that the pathway B is not even available for the green emission energetically.

The similar conclusion about the pathways is reached by examining the excitation power dependence of the green and red emission band intensity. In Figure 3, we show the emission spectra obtained at varying excitation power (Figure 3a) and the results of analyses (Figure 3b and 3c). In the log-log plots for the band intensity as a function of excitation power (Figure 3b), the slopes lie between 1 and 2, which indicates that the upconversion processes for the red and green emission band both involve two-photon absorption at 980 nm. The reason why they are not exactly 2 (integer) is associated with the presence of the "real" intermediate states from which competing decay channels other than upconversion are available.[5] Also, these log-log plots are bimodal with the slopes of *ca.* 2 in the low power region ($P < 50$ W/cm^2) to *ca.* 1 in the high power regime ($P > 50$ W/cm^2). Such behavior was previously observed and explained to be due to the saturated absorption of the sensitizer (Yb^{3+}).[22,23] In other words, at high power, the saturated sensitizer keeps the acceptor (Er^{3+}) in the excited state rather than in the ground state and only one subsequent energy transfer is required to bring it to emitting states. As a result, the slope of the power dependence in the high power region of the log-log plot converges to 1 regardless of the number of energy transfer steps involved.[22] With the power dependences of individual bands, however, there seems to be no further information. Instead, we note that, by plotting the ratio of the green to red intensity as a function of power, a piece of new evidence about the partitioning between two pathways (A and B) can be extracted (Figure 3c). The intensity of an emission band is proportional to the *n*th power of excitation power,

$$I_{em} = \alpha P^{n} \tag{1}$$

where α is the proportionality constant characteristic of a given transition, and P is the excitation power. If we apply this relation to the green and the red band, the ratio is

$$\frac{I_g}{I_r} = \frac{\alpha_g}{\alpha_r} P^{(n_g - n_r)} \equiv \beta P^{\Delta n} \tag{2}$$

where the subscripts, *g* and *r*, designate “green” and “red” emission, respectively. In this relation, if the red emission results from the pathway A, $\Delta n = 0$ because the “photo-induced” processes (excitation) that lead to the green and red emission are the same. In other words, the ratio becomes a constant (β) without any power dependence. On the other hand, if the red emission were the outcome of the pathway B, Δn is not necessarily 0, and the I_g/I_r would vary with excitation power. In fact, what we observed was a decaying profile for I_g/I_r as shown in Figure 3c, supporting the idea that the pathways are different indeed between the green and red emission. Again, this leads to the conclusion that the red emission results from pathway B. However, the situation is not that simple. Interestingly, we found a long tail which converges to a constant ($I_g/I_r = \sim 0.4$), and being invariant ($\Delta n = 0$) over the high power range probably means that the pathway A is predominant in this regime. If so, we might be able to explain the switching from the pathway B to A as follows. In the low power limit, most population of $^4I_{11/2}$ generated after the first energy transfer will have chances to decay to the lower level $^4I_{13/2}$. Obviously, this is due to the low level of photon flux. On the other hand, the high level of photon flux would force the population of $^4I_{11/2}$ to be excited further rather than allow it to decay to the lower level ($^4I_{13/2}$). This causes that pathway A appear to be open as the excitation power increases, and becomes predominant in the high power limit. However, the observation that the ratio (I_g/I_r) converges to 0.4, and the notion that it involves pathway A are, in fact, contradictory to each other considering the result of 488-nm excitation shown in Figure 2. In 488-nm excitation scheme which is equivalent to the pathway A, the red emission band disappeared nearly completely, and therefore, the ratio (I_g/I_r) should be much higher than 1. In fact, we never observed a spectrum where the red band is smaller than the green bands with 980-nm excitation. Then we should accept the idea that the pathway B is still favored by UCNPs for the red emission even at the high power regime. Then why do the ratio converge to 0.4 but not to 0 in eq. (2) for high power (P)? It is most likely to be due to the saturation of Yb^{3+} absorption that results in the slope of 1 for both the green and red emission as mentioned above, and hence $\Delta n = 0$ (with $\beta = 0.4$) in eq. (2).[22,23]

The different pathways between the green (A) and red (B) bands result in different photophysical kinetics associated with upconversion. We employed a Nd:YAG-pumped OPO (optical parametric oscillator) which generates 980-nm laser pulse to excite UCNPs at the nanosecond scale and measured the time-resolved emission for the bands centered at 525, 540, or 655 nm. As shown in Figure 4, all the emission bands contain rises as well as decay components. The rises in the time-resolved profiles usually reflect the time scale of the population of emitting states. For UCNPs, in particular, the information about the upconversion mechanisms prior to the emission is embedded in those rise components. The time scale of population of the emitting states $^{2}H_{11/2}$, $^{4}S_{3/2}$, and $^{4}F_{9/2}$, are 23, 30, and 60 μs, respectively. The two emitting states for the green bands are populated more quickly than that for the red band, which is highlighted in Figure 4 (bottom right). This must be the consequence of the differences in the pathways between the green and the red emission in the upconversion process. Interestingly, no rise component is observed in the temporal profiles obtained by 488-nm direct excitation (Figure S3), which indicates that the dynamic information on the upconversion processes (i.e., time scale of the energy transfers and the non-radiative multiphonon relaxations) are indeed contained in the rise components in 980-nm excitation.

Conclusions

In summary, we provided convincing evidence supporting the hypothesis that the red emission of UCNPs (β-$NaYF_4$:Yb^{3+}, Er^{3+}/$NaYF_4$) results from the pathway B exclusively by (1) comparing the one-photon (488 nm) and two-photon upconversion (980 nm) emission spectra, (2) examining the power dependence of upconversion emission, and (3) estimating the time scales of photophysical steps by time-resolved emission measurements. The mechanistic studies on the upconversion process should be crucial for understanding, designing and controlling the remarkable optical properties of UCNPs.

Acknowledgements

K.T.L. was supported by the GIST Specialized Research (GSR) Project (K05030), Bio Imaging Research Center of GIST (K04784), the Basic Science Research Program (NRF-2013R1A1A1058451) of NRF, and the Brain Korea 21 Plus (10Z20130012677). H.L. was supported by the GSR (K05040) of GIST, the Basic Science Research Program (NRF-2014R1A1A2056255), and the Integrative Aging Research Center of GIST. T.H. acknowledges the financial support by the Research Center Program of the Institute for Basic Science (IBS). Y.D.S. was supported by KRICT (SI-1408, KK0904-02, OASIS Project), the Public Welfare & Safety Research Program (2011-0020957) of NRF, ICT, and Future Planning (MSIP, Korea). H.M.K. acknowledges the financial support by the Basic Science Research Program of NRF (NRF-2013R1A1A1008710).

References

1 F. Auzel, *Chem. Rev.*, 2004, **104**, 139.

2 M. Haase and H. Schäfer, *Angew. Chem. Int. Ed.*, 2011, **50**, 5808.

3 F. Wang, D. Banerjee, Y. Liu, X. Chen and X. Liu, *Analyst*, 2010, **135**, 1839.

4 G. Chen and G. Han, *Theranostics*, 2013, **3**, 289.

5 G. Chen, H. Qiu, P. N. Prasad and X. Chen, *Chem. Rev.*, 2014, **114**, 5161.

6 Y. I. Park, J. H. Kim, K. T. Lee, K.-S. Jeon, H. Bin Na, J. H. Yu, H. M. Kim, N. Lee, S. H. Choi, S.-I. Baik, H. Kim, S. P. Park, B.-J. Park, Y. W. Kim, S. H. Lee, S.-Y. Yoon, I. C. Song, W. K. Moon, Y. D. Suh and T. Hyeon, *Adv. Mater.*, 2009, **21**, 4467.

7 S. H. Nam, Y. M. Bae, Y. I. Park, J. H. Kim, H. M. Kim, J. S. Choi, K. T. Lee, T. Hyeon and Y. D. Suh, *Angew. Chem. Int. Ed.*, 2011, **50**, 6093.

8 Y. M. Bae, Y. I. Park, S. H. Nam, J. H. Kim, K. Lee, H. M. Kim, B. Yoo, J. S. Choi, K. T. Lee, T. Hyeon and Y. D. Suh, *Biomaterials*, 2012, **33**, 9080.

9 S. Wu, G. Han, D. J. Milliron, S. Aloni, V. Altoe, D. V. Talapin, B. E. Cohen and P. J. Schuck, *Proc. Natl. Acad. Sci. U. S. A.*, 2009, **106**, 10917.

10 Y. I. Park, H. M. Kim, J. H. Kim, K. C. Moon, B. Yoo, K. T. Lee, N. Lee, Y. Choi, W. Park, D. Ling, K. Na, W. K. Moon, S. H. Choi, H. S. Park, S.-Y. Yoon, Y. D. Suh, S. H. Lee and T. Hyeon, *Adv. Mater.*, 2012, **24**, 5755.

11 H. S. Mader, P. Kele, S. M. Saleh and O. S. Wolfbeis, *Curr. Opin. Chem. Biol.*, 2010, **14**, 582.

12 Y. I. Park, S. H. Nam, J. H. Kim, Y. M. Bae, B. Yoo, H. M. Kim, K.-S. Jeon, H. S. Park, J. S. Choi, K. T. Lee, Y. D. Suh and T. Hyeon, *J. Phys. Chem. C*, 2013, **117**, 2239.

13 H.-X. Mai, Y.-W. Zhang, L.-D. Sun and C.-H. Yan, *J. Phys. Chem. C*, 2007, **111**, 13721.

14 S. F. Lim, W. S. Ryu and R. H. Austin, *Opt. Express*, 2010, **18**, 2309.

15 Y. Wang, L. Tu, J. Zhao, Y. Sun, X. Kong and H. Zhang, *J. Phys. Chem. C*, 2009, **113**, 7164.

16 D. Li, B. Dong, X. Bai, Y. Wang and H. Song, *J. Phys. Chem. C*, 2010, 114, 8219.

17 J. Shan, M. Uddi, R. Wei, N. Yao and Y. Ju, *J. Phys. Chem. C*, 2010, **114**, 2452.

18 J. Zhao, Y. Sun, X. Kong, L. Tian, Y. Wang, L. Tu, J. Zhao and H. Zhang, *J. Phys. Chem. B*, 2008, **112**, 15666.

19 W. Niu, S. Wu, S. Zhang, J. Li and L. Li, *Dalton Trans.*, 2011, **40**, 3305.

20 J.-C. Boyer, L. A. Cuccia and J. A. Capobianco, *Nano Lett.*, 2007, **7**, 847.

21 R. B. Anderson, S. J. Smith, P. S. May and M. T. Berry, *J. Phys. Chem. Lett.*, 2014, **5**, 36.

22 J. F. Suyver, A. Aebischer, S. García-Revilla, P. Gerner and H. U. Güdel, *Phys. Rev. B*, 2005, **71**, 125123.

23 Y. Y. Zhang, L. W. Yang, H. L. Han and J. X. Zhong, *Opt. Commun.*, 2009, **282**, 2857.

.

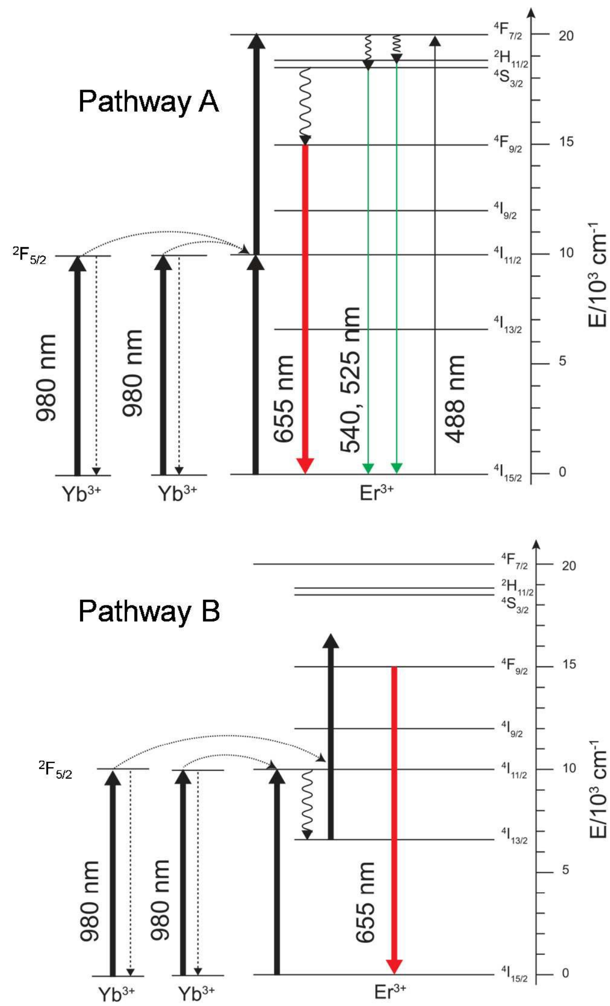

Figure 1. The energy diagram of UCNPs ($NaYF_4$:Yb^{3+},Er^{3+} or $NaYF_4$:Yb^{3+},Er^{3+}/$NaYF_4$) and two possible upconversion pathway. The black arrows represent the relevant photophysical steps: (1) 980-nm excitation of Yb^{3+} (with "980 nm"), (2) 488-nm direct excitation of Er^{3+} (with "488 nm"), (3) the energy transfer from Yb^{3+} to Er^{3+} (dotted and curved), (4) excitation of Er^{3+} (bare solid), (5) non-radiative relaxation of Yb^{3+} (dotted), and (6) multi-phonon relaxation of Er^{3+} (wavy). The colored arrows represent upconversion emission from the excited states of Er^{3+}, centered at 525 nm (green, right), 540 nm (green, left), and 655 nm (red). Pathway A designates the upconversion process where the excitation to the $^4F_{7/2}$ precedes the multi-phonon relaxation to the emitting states ($^2H_{11/2}$, $^4S_{3/2}$, and $^4F_{9/2}$). In the pathway B, on the other hand, the multiphonon relaxation occurs prior to the second excitation to the emitting state for the red band ($^4F_{9/2}$).

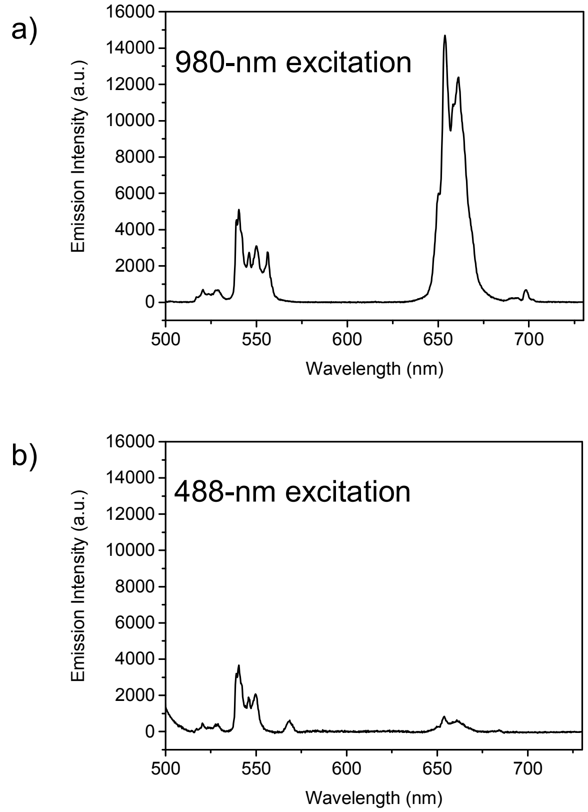

Figure 2. Emission spectra of UCNPs (hexagonal β-$NaYF_4$:Yb^{3+},Er^{3+}/$NaYF_4$ core/shell) in *n*-hexane (100 nM) obtained by (a) upconversion with 980-nm laser and (b) one-photon direct excitation of Er^{3+} with 488-nm laser.

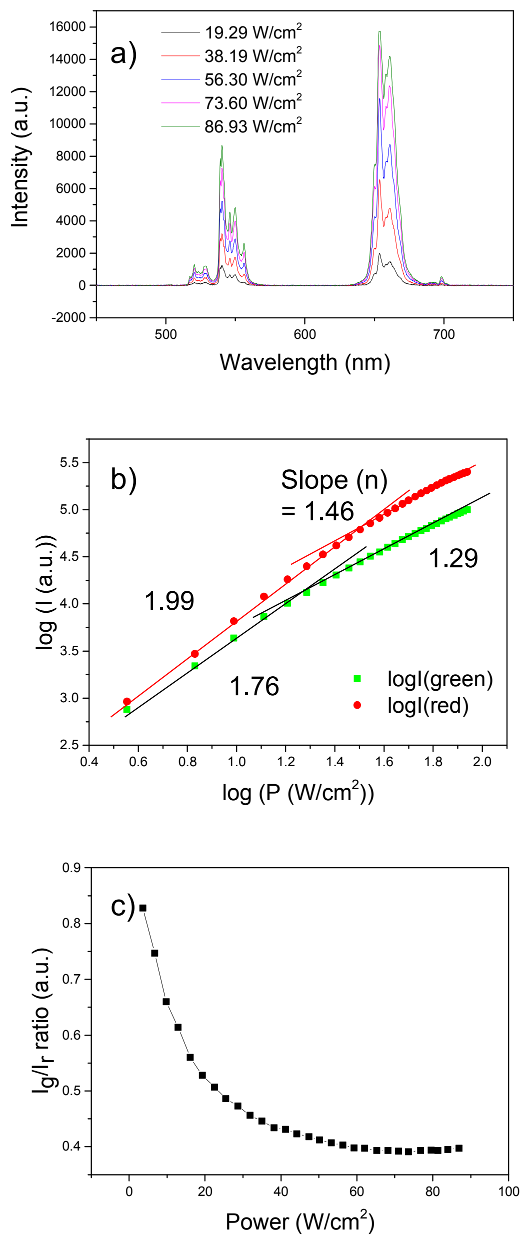

Figure 3. (a) The emission spectra of UCNPs at various excitation powers. (b) The log-log plot of the green (centered at 525 and 540 nm) and red emission (centered at 655 nm) intensity (band area) as a function of the laser power. Also shown are the slopes of the linear fits. (c) The ratio of emission intensity (green-to-red) as a function of the excitation power.

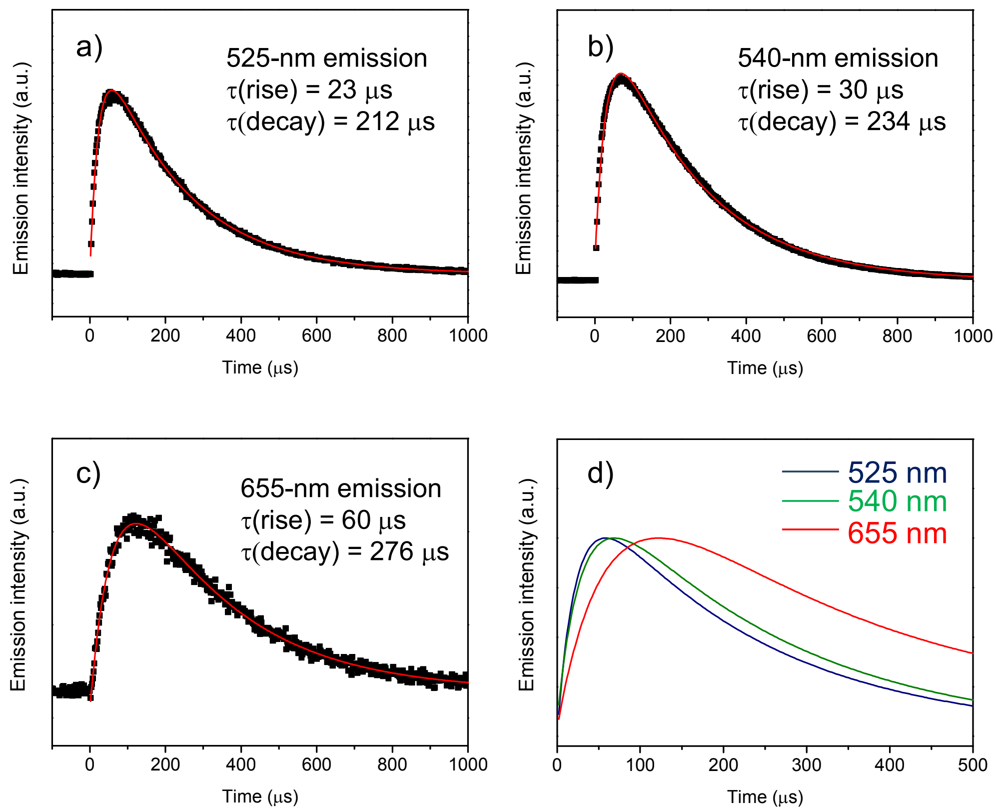

Figure 4. Time-resolved emission spectra of UCNPs monitored at different wavelength (525, 540 nm for green band, and 655 nm for the red band) upon 980-nm excitation and the overlay of their best fits. The time constants were obtained by fitting the experimental curves to $I(t) = A \exp(-t/\tau(\text{decay})) - B \exp(-t/\tau(\text{rise})) + \text{const.}$, where $A, B > 0$. The overlay highlights the differences in rise components between the green and red emission, which shows that the latter is ca. 2–3 times slower than the former bands.

TOC graphics

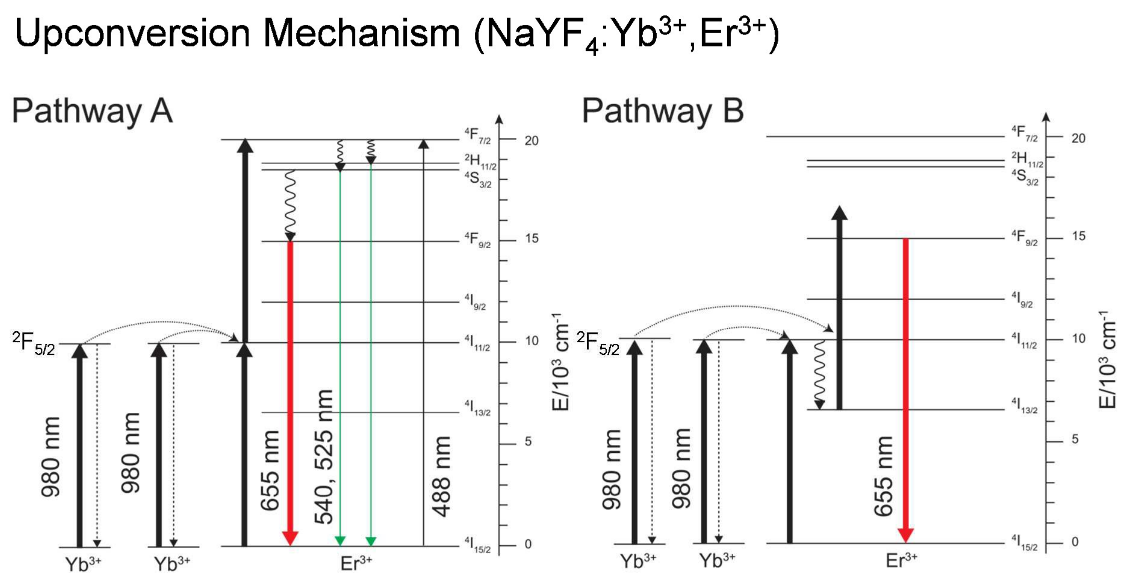

It has been suggested that there are two photophysical pathways for the red emission of lanthanide-doped UCNPs ($NaYF_4$:Yb^{3+},Er^{3+}/$NaYF_4$) but, in fact, it turns out that only one of them is predominant over a wide range of excitation power.